Fullerene Fragments

DOI: 10.1002/anie.201309672

Electron Transfer in a Supramolecular Associate of a Fullerene Fragment**

María Gallego, Joaquín Calbo, Juan Aragó, Rafael M. Krick Calderon, Fernando H. Liquido, Takahiro Iwamoto, Allison K. Greene, Edward A. Jackson, Emilio M. Pérez, Enrique Ortí, Dirk M. Guldi,* Lawrence T. Scott,* and Nazario Martín**

Abstract: *Herein, we investigate the association of a fullerene fragment, hemifullerene $C_{30}H_{12}$, with an electron-donating bowl-shaped tetrathiafulvalene derivative (truxTTF). UV/Vis titrations and DFT calculations support formation of the supramolecular complex, for which an association constant of log $K_a = 3.6 \pm 0.3$ in $CHCl_3$ at room temperature is calculated. Remarkably, electron transfer from truxTTF to $C_{30}H_{12}$ to form the fully charge-separated species takes place upon irradiation of the associate with light, constituting the first example in which a fullerene fragment mimics the electron-accepting behavior of fullerenes within a supramolecular complex.*

The different nanoforms of carbon,[1] namely fullerenes,[2] carbon nanotubes,[3] and graphene,[4] each present distinct extraordinary properties that have attracted a great deal of attention in different areas of research. Fullerenes, in particular C_{60} and its derivatives, have been thoroughly studied as electron acceptors in fundamental investigations of photoinduced electron transfer (PET) processes, combined with a variety of electron donors in covalent and noncovalent dyads.[5] From an application point of view, C_{60} and C_{70} derivatives are by far the most commonly utilized n-type semiconducting materials in organic solar cells.[6] In the case of carbon nanotubes, both their mechanical and optoelectronic properties have been exploited to construct a variety of devices, including field-effect transistors and sensors.[7] Finally, graphene is currently considered to have the potential to be the "balm of Fierabras" of carbon-based technologies. Transparent electrodes,[8] extremely sensitive sensors,[9] supercapacitors,[10] and lightweight high-performance materials[11] have all been postulated as potential applications of graphene.[12]

Molecular fragments of these carbon nanoforms[13] can serve as model systems for their investigation, with the added value of their synthetic availability in pure form with a well-defined molecular structure. The coordination of metal cations by fullerene fragments has been thoroughly studied, and they have also been used frequently to construct receptors for fullerenes,[14] but their binding by other organic hosts has not been investigated thus far. Herein, we present the first insights into the supramolecular association of a fullerene fragment (hemifullerene, $C_{30}H_{12}$) with a bowl-shaped electron donor molecule, based on a truxene core to which three dithiole rings are covalently attached (truxTTF).[15] The chemical structures of $C_{30}H_{12}$ and truxTTF are shown in Figure 1 a.

Several syntheses[16] and two crystal structures[17] of hemifullerene $C_{30}H_{12}$ were reported a few years ago. In the solid state, two polymorphs were found, each of which showed a different packing motif, originating from the interaction between the $C_{30}H_{12}$ molecules. In the trigonal polymorph, bowl-in-bowl columnar stacks were found, an arrangement in which π–π interactions are maximized (Figure 1 b). In the orthorhombic polymorph, each hemifullerene inserts one of its six-membered rings into the cavity of a neighboring molecule, forming dimers in which both CH–π and π–π interactions play a primary role (Figure 1 c). On the other hand, in truxTTF, a bowl-in-bowl arrangement is prevented

[*] M. Gallego, Prof. Dr. N. Martín
Departamento de Química Orgánica, Fac. C.C. Químicas
Universidad Complutense de Madrid
Av. Complutense s/n, 28040 Madrid (Spain)
E-mail: nazmar@quim.ucm.es
Homepage: http://www.ucm.es/info/fullerene/

J. Calbo, Dr. J. Aragó, Prof. Dr. E. Ortí
Instituto de Ciencia Molecular, Universidad de Valencia
46980 Paterna (Spain)
E-mail: enrique.orti@uv.es

R. M. Krick Calderon, Prof. Dr. D. M. Guldi
Department of Chemistry and Pharmacy & Interdisciplinary Center for Molecular Materials (ICMM), Friedrich-Alexander-Universität Erlangen-Nürnberg, Egerlandstraße 3, 91058 Erlangen (Germany)
E-mail: guldi@chemie.uni-erlangen.de

F. H. Liquido, T. Iwamoto, A. K. Greene, E. A. Jackson, Prof. Dr. L. T. Scott
Merkert Chemistry Center, Boston College
Chestnut Hill, MA-02467-3860 (USA)
E-mail: lawrence.scott@bc.edu

Dr. E. M. Pérez, Prof. Dr. N. Martín
IMDEA-nanociencia, C/Faraday 9, Ciudad Universitaria de Cantoblanco, 28049 Madrid (Spain)

[**] This work was supported by the ERC (AdG Chirallcarbon ERC-2012-ADG_20120216), the MINECO of Spain (CTQ2011-24652, CTQ2011-25714, CTQ2012-31914, PIB2010JP-00196, and Consolider-Ingenio CSD2007-00010), the CAM (MADRISOLAR-2 S2009/PPQ-1533), the Generalitat Valenciana (PROMETEO/2012/053), the European FEDER funds (CTQ2012-31914), and the Bavarian Initiative "Solar Technologies go Hybrid". E.M.P. is thankful to the MINECO for a Ramón y Cajal research fellowship. M.G and J.C. acknowledge the Spanish Ministry of Education, Culture and Sport (MECD) for FPU grants. T.I. is grateful to The Kyoto University Foundation for an overseas study fellowship.

Supporting information for this article is available on the WWW under http://dx.doi.org/10.1002/anie.201309672.

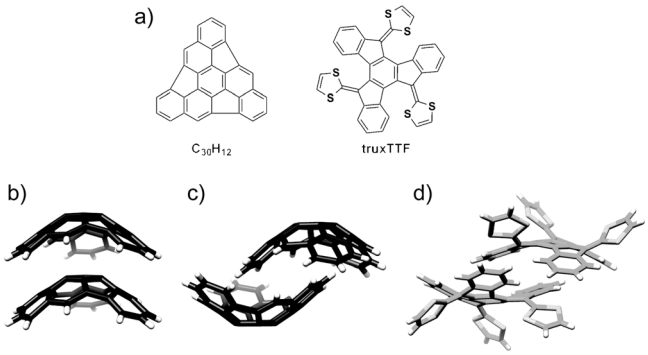

Figure 1. a) Chemical structures of hemifullerene $C_{30}H_{12}$ and truxTTF. b,c) Structures of the dimers formed by $C_{30}H_{12}$ (C black) in its trigonal and orthorhombic crystal polymorphs, respectively. d) Structure of the dimers formed by truxTTF (C gray, S light gray) in its crystal packing.

by the protruding dithiole rings and, consequently, only the dimeric form in which one of the aromatic rings of each monomer is placed inside the cavity of the other is found (Figure 1 d). Because of their concave shape, both $C_{30}H_{12}$ and truxTTF are inherently chiral,[18] consequently, each is obtained as a racemic mixture of two enantiomers.

Considering the ability of truxTTF to associate fullerenes,[15,19] and its electron-donating character, we reasoned that it should also be able to bind $C_{30}H_{12}$, forming heteromolecular bowl–bowl complexes. To explore this possibility, we first carried out density functional theory (DFT) calculations on four different supramolecular truxTTF·$C_{30}H_{12}$ models, which were rationally constructed from the crystallographic information on both $C_{30}H_{12}$ and truxTTF. All of the models proposed were fully optimized using the revPBE0-D3 functional,[20] which is capable of capturing the dispersion effects and is one of the best density functionals to accurately describe supramolecular complexes governed by π–π interactions.[21] The revPBE0-D3 functional has been successfully applied in the structural and energetic characterization of related supramolecular nanoarchitectures between a tetrathiafulvalene derivative and a graphene sheet model.[22]

Figure 2 displays the minimum-energy structures (**1**–**4**) computed for the truxTTF·$C_{30}H_{12}$ heterodimer at the revPBE0-D3/cc-pVTZ level. The most relevant intermolecular distances in **1**–**4** are given in Figure S1 in the Supporting Information. The truxTTF·C_{60} associate was also calculated at the same level of theory (Figure S2). In structures **1** and **2**, the convex surface of the $C_{30}H_{12}$ bowl perfectly matches the two concave cavities of the truxTTF host; that is, either through the cavity formed by the carbon backbone (structure **1**) or through the cavity formed by the central benzene ring and the three dithiole rings (structure **2**). Both structures can be thus seen as bowl-in-bowl arrangements where π–π interactions are maximized. The concave cavities of truxTTF and $C_{30}H_{12}$ can also interact, giving rise to heterodimers in which either a benzene or a dithiole ring of the truxTTF molecule is placed inside the concave cavity of the hemifullerene bowl (structures **3** and **4**, respectively). The optimized heterodimeric structures **1**–**4** all show close intermolecular contacts in the 2.5–3.7 Å range (Figure S1), which is indicative of the positive noncovalent interaction between both bowls.

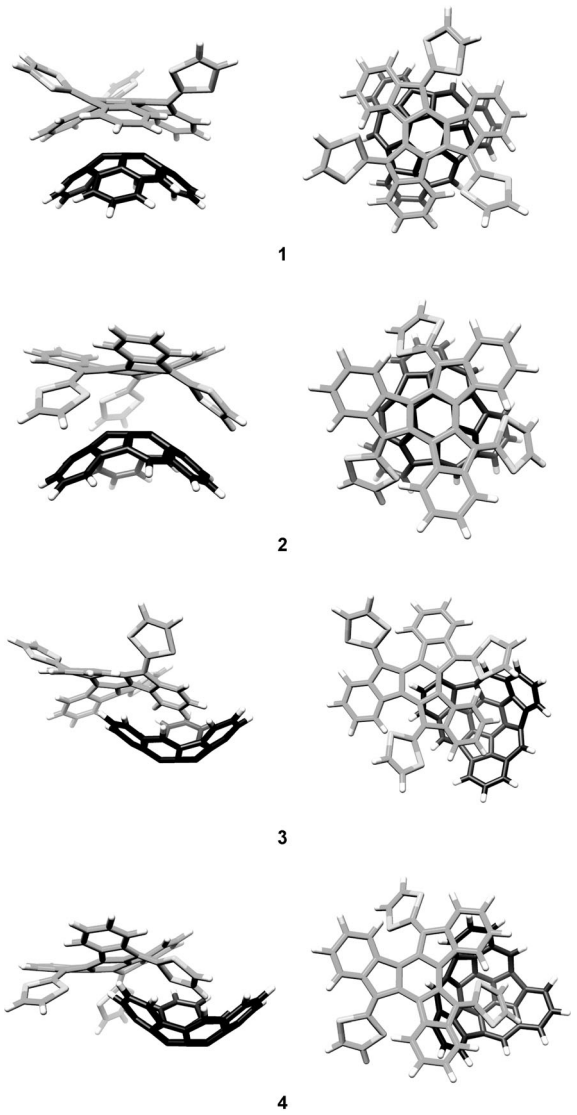

Figure 2. Minimum-energy structures (**1**–**4**) computed for the truxTTF·$C_{30}H_{12}$ heterodimer at the revPBE0-D3/cc-pVTZ level. For truxTTF: C gray, S light gray, H white. For $C_{30}H_{12}$: C black, H white.

To assess the strength of the interaction between the truxTTF and $C_{30}H_{12}$ bowls, association energies for the previously optimized heterodimers were also calculated at revPBE0-D3/cc-pVTZ. The four supramolecular structures **1**–**4** exhibit significant gas-phase association energies, ranging from −21.0 and −19.4 kcal mol^{-1} for **1** and **2**, respectively, to −25.2 and −28.5 kcal mol^{-1} for **3** and **4**, respectively. The bowl-in-bowl arrangements are therefore significantly less stable than the staggered ones. The truxTTF·C_{60} model system, for which we have experimentally calculated association constants in the range of log $K_a = 3$–4 in a variety of solvents at room temperature,[15,19] presents an association energy of −22.1 kcal mol^{-1}, which is very close to that computed for structure **1**, owing to the similarity in the concave–convex interaction.

The electronic properties of the truxTTF·$C_{30}H_{12}$ associate have also been theoretically investigated. Figure S3 a sketches

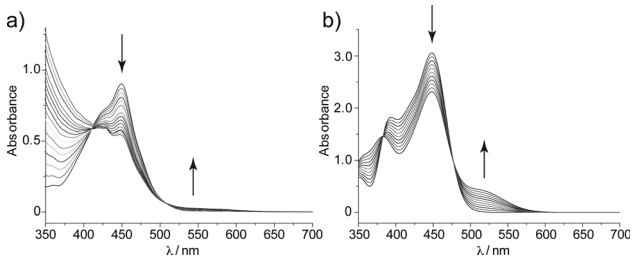

Figure 3. a) Experimental UV/Vis spectra, as obtained during the titration of truxTTF (1.7×10^{-4} M) with $C_{30}H_{12}$ (0.8×10^{-3} M) in $CHCl_3$ at room temperature. Each addition corresponds to 0.2 equiv. b) TDDFT simulation of the absorption spectra of truxTTF as the ratio of truxTTF·$C_{30}H_{12}$ increases from 0 to 100% (B3LYP/cc-pVDZ calculations including $CHCl_3$ as solvent).

the highest occupied (HOMO-2 to HOMO) and lowest unoccupied (LUMO to LUMO + 4) molecular orbitals computed at the revPBE0-D3/cc-pVTZ level for the most stable structure (**4**) of truxTTF·$C_{30}H_{12}$. Similar molecular orbital distributions are found for the rest of supramolecular structures **1**–**3** (Figure S3b). The HOMO, HOMO-1, and HOMO-2 spread over the electron-donating truxTTF moiety. In contrast, the LUMO, LUMO + 1, and LUMO + 2 are localized on the electron-accepting $C_{30}H_{12}$ bowl, with LUMO + 1 and LUMO + 2 being almost degenerate. Above LUMO + 2, LUMO + 3 and LUMO + 4 are again concentrated on the truxTTF bowl. The nature and energies calculated for the HOMOs and LUMOs of truxTTF·$C_{30}H_{12}$ therefore suggest that photoinduced charge-transfer processes from truxTTF to $C_{30}H_{12}$ should take place in the UV/Vis range.

Encouraged by the results of the theoretical calculations, we titrated truxTTF (1.7×10^{-4} M) with $C_{30}H_{12}$ (0.8×10^{-3} M) in $CHCl_3$ at room temperature. The electronic absorption spectra resulting from this titration experiment are depicted in Figure 3a. We observed a decrease in the intensity of the truxTTF absorption at $\lambda = 450$ nm, accompanied by the increase of a broad charge-transfer band in the 500–600 nm region. These spectral changes are analogous to those found in the titration of truxTTF vs. C_{60}, albeit with a significantly less intense charge-transfer feature.[19] The results of three separate titration experiments were analyzed with Reactlab Equilibria software, affording a binding constant of $\log K_a = 3.6 \pm 0.3$.

To gain more insight into the electronic nature of the absorption bands observed experimentally, and their evolution during the titration experiment, the lowest-energy singlet excited states (S_n) of the truxTTF·$C_{30}H_{12}$ heterodimer and of isolated truxTTF were computed using the time-dependent DFT (TDDFT) approach, taking into account the solvent effects (see the Computational Details in the Supporting Information). Only the results obtained for the most stable structure (**4**) of truxTTF·$C_{30}H_{12}$ are discussed. TDDFT calculations predict the first two excited states S_1 and S_2 at 537 nm (2.31 eV) and 516 nm (2.40 eV) above the ground state S_0 with moderate oscillator strengths (*f*) of 0.036 and 0.046, respectively. The $S_0\rightarrow S_1$ and $S_0\rightarrow S_2$ electronic transitions are mainly described by one-electron promotions from the HOMO to the LUMO and LUMO + 1, respectively. These transitions therefore imply a charge transfer from the electron-donor, truxTTF, where the HOMO is located, to the electron-acceptor, $C_{30}H_{12}$, where the LUMO and LUMO + 1 are spread (Figure S3a), and are the major contribution to the charge-transfer band experimentally recorded in the 500–600 nm range. Other charge-transfer transitions are computed around 500 nm, but they are less intense (Supporting Information, Table S1). At higher energies, the S_9 (454 nm, 2.73 eV), S_{10} (452 nm, 2.75 eV), and S_{11} (445 nm, 2.78 eV) states are calculated to be very close in energy and present higher oscillator strengths (0.178, 0.178, and 0.093, respectively). The $S_0\rightarrow S_9$, $S_0\rightarrow S_{10}$, and $S_0\rightarrow S_{11}$ electronic transitions mainly originate from the HOMO, HOMO-1→LUMO + 3, LUMO + 4 one-electron excitations localized on truxTTF (Figure S3a), and give rise to the absorption band observed at 450 nm. The oscillator strengths calculated for these transitions are significantly smaller than those computed for isolated truxTTF (0.277, 0.320, and 0.145, respectively).

A TDDFT simulation of the absorption spectra of the truxTTF chromophore as the amount of truxTTF·$C_{30}H_{12}$ increases from 0 (spectrum of truxTTF) to 100% is shown in Figure 3b. The simulation clearly reveals that the truxTTF band decreases in intensity as truxTTF·$C_{30}H_{12}$ forms. This decrease is due to the smaller oscillator strengths computed for the truxTTF-centered transitions in the truxTTF·$C_{30}H_{12}$ complex. The charge-transfer band associated with the formation of truxTTF·$C_{30}H_{12}$ simultaneously increases in intensity. The theoretical simulation is in notable agreement with the experimental evolution of the absorption spectra, and supports the formation of the supramolecular donor–acceptor truxTTF·$C_{30}H_{12}$ heterodimer.

In addition to the ground-state interactions, we turned to pump probe absorption measurements to unravel the processes following photoexcitation of truxTTF·$C_{30}H_{12}$ and their references, truxTTF and $C_{30}H_{12}$. Upon 470 nm excitation of truxTTF, a new transient immediately develops (Figure S4). Characteristics of the latter are a marked maximum in the visible at 530 nm and a broad, featureless transition that spans all throughout the near infrared. Furthermore, a marked ground-state bleaching is observed around 450 nm. This excited state decays rapidly, as in other sulfur-rich electron donors, with a lifetime of only 1.0 ± 0.1 ps. The short lifetime is rationalized by the presence of the sulfur atoms, with a strong second-order vibronic spin-orbit coupling, as it transforms into a much weaker absorbing state, for which a lifetime of 20 ± 1 ps is detected.

For $C_{30}H_{12}$, the singlet and triplet excited states upon 387 nm excitation include transient maxima at 515 and 586 nm(Figure S5). These reflect the singlet excited state that decays within 11 ns through intersystem crossing to the energetically low-lying triplet excited state.

Following 470 nm photoexcitation of truxTTF·$C_{30}H_{12}$ (1:5 ratio), the differential absorption changes are dominated by truxTTF-centered features (Figure 4). Within approximately 1.5 ± 0.5 ps, the latter give place, however, to a new transient with characteristics that include maxima at 440, 475, 495, 530 (sh), and 615 nm, as well as a minimum at 450 nm. Neither photoexcited $C_{30}H_{12}$ nor photoexcited truxTTF exhibit differ-

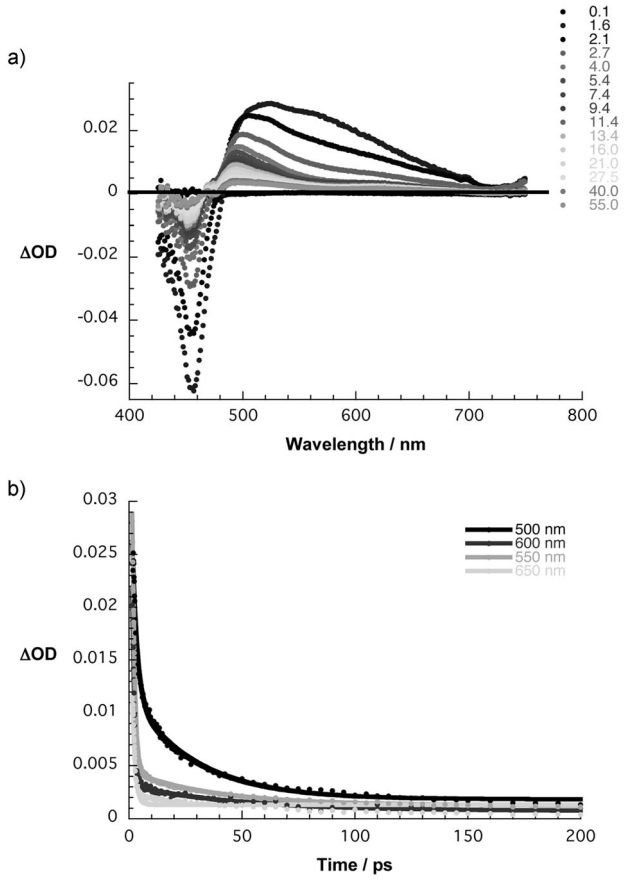

Figure 4. a) Differential absorption spectra (visible) obtained upon femtosecond pump probe experiments (470 nm) of truxTTF·$C_{30}H_{12}$ (1:5 ratio) in chlorobenzene with time delays of 0.1–55.0 ps at room temperature. b) Time absorption profiles of the spectra shown in (a) at 500 (black spectrum), 550 (gray spectrum), 600 (dark-gray spectrum), and 650 nm (light-gray spectrum) monitoring the charge transfer.

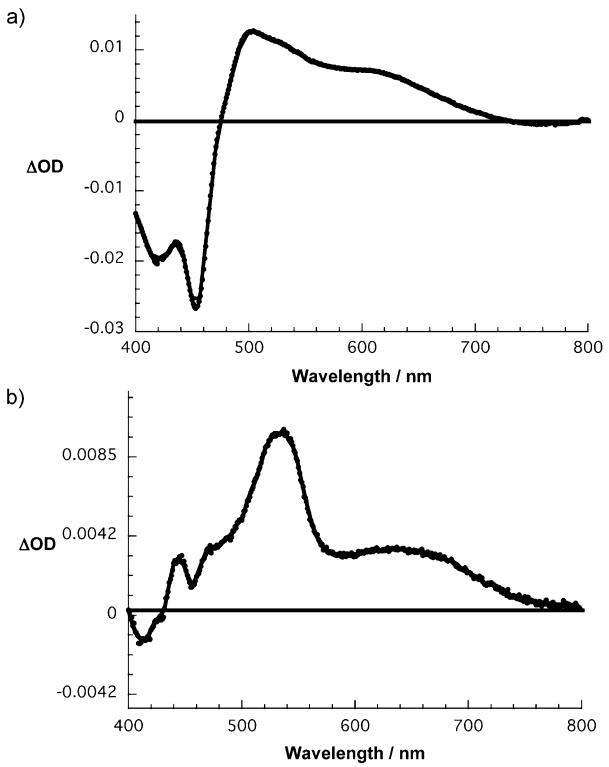

Figure 5. Differential absorption spectra (visible) obtained upon spectroelectrochemical oxidation of truxTTF (a) and reduction of $C_{30}H_{12}$ (b) in deoxygenated *ortho*-dichlorobenzene containing $TBAPF_6$ (0.1 M) with potentials vs. Ag wire of +0.8 and −1.0 V, respectively.

ential absorption changes that bear any significant resemblance to these data (Figure S4 and S5). Thus, a tentative assignment of these features implies the formation of a charge-separated state.

Support for this interpretation comes from spectroelectrochemical oxidation and reduction experiments with truxTTF and $C_{30}H_{12}$ in *ortho*-dichlorobenzene, respectively. For the former, upon applying a potential of +0.8 V versus Ag wire, maxima at 500 and 615 nm and a minimum at 450 nm are noted (Figure 5a). Importantly, resetting the potential back to 0 V led to a quantitative recovery of the starting spectrum. In the context of the latter, a potential of −1.0 V was chosen, and the differential absorption changes for the reduced $C_{30}H_{12}$ include maxima at 445, 475, 530, and 640 nm, which are accompanied by a 455 nm minimum (Figure 5b). Again, these changes were reversed upon resetting the applied potential back to 0 V. As such, the differential absorption changes upon photoexciting truxTTF·$C_{30}H_{12}$ (Figure 4) are in sound agreement with the superimposition of the spectroelectrochemically initiated oxidation and reduction of the truxTTF and hemifullerene, respectively. From multiwavelength analyses we derive rate constants of 6.6×10^{11} and $1.0\times10^{10}\ s^{-1}$ for the charge separation and charge recombination dynamics, respectively.

To better understand the spectroelectrochemical data recorded for the truxTTF and $C_{30}H_{12}$ fragments, the theoretical absorption spectra of the singly oxidized truxTTF$^{\bullet+}$ and singly reduced $C_{30}H_{12}^{\bullet-}$species were computed. The spectra calculated for the neutral species were subtracted from the spectra of the oxidized/reduced systems to obtain a theoretical simulation of the differential absorption spectra (Figure S6). For the truxTTF fragment, the predicted spectrum (Figure S6a) is in excellent agreement with the experimental spectrum (Figure 5a). The long tail over 550–800 nm originates from electron promotions from high-energy, doubly occupied molecular orbitals to the single-occupied molecular orbital (SOMO) (doublet states D_5 to D_9). The peak observed at 500 nm is due to higher-energy excitations (states D_{12} to D_{15}), where SOMO→LUMOs transitions are involved. The steep slope experimentally recorded at around 480 nm is nicely reproduced by the theoretical simulation and originates from the proximity in energy of the intense excitation to the doublet state D_{17} in the cation and the excitation to the singlet state S_2 in the neutral species. The two-peak bleaching in the 400–450 nm region is due to the intense transitions (S_5–S_6 and S_7–S_8) of neutral truxTTF counterbalanced between them by the intense doublet excitation (D_{24}) in the cation. For the hemifullerene fragment, the theoretical simulation (Figure S6b) is in worse agreement with the experimental spectrum (Figure 5b) because the most intense band is

calculated too high in energy. The lower-energy band appearing at 600–700 nm corresponds to doublet excitations (D_3–D_5) from the SOMO to higher-unoccupied molecular orbitals. The near-degeneracy of the LUMOs in neutral $C_{30}H_{12}$ is the origin of these low-energy transitions. Otherwise, the main features experimentally observed above 420 nm are assigned to doublet transitions (D_8 to D_{20}) implying electron excitations from doubly occupied molecular orbitals to the SOMO.

In summary, we have corroborated the association of a fullerene fragment, namely hemifullerene $C_{30}H_{12}$, with a bowl-shaped electron-donor, truxTTF. The association was investigated experimentally through UV/Vis titrations. To this end, changes in the absorption spectra, most notably a decrease in the truxTTF absorption and the formation of a weak charge transfer band, are clearly indicative for the truxTTF·$C_{30}H_{12}$ heterodimer in solution. Quantitatively, we calculated a binding constant of $\log K_a = 3.6 \pm 0.3$ in $CHCl_3$ at room temperature, which is comparable to that found for the association of truxTTF with C_{60}. Calculations at the revPBE0-D3/cc-pVTZ level of theory supported the noncovalent interactions between truxTTF and $C_{30}H_{12}$; providing insight into the possible structure of the heterodimer and the nature of the changes observed during the UV/Vis titration.

Remarkably, femtosecond pump-probe experiments reveal the formation of a transient species that corresponds to a charge-separated truxTTF$^{\bullet+}$·$C_{30}H_{12}^{\bullet-}$ state. Overall, the latter assignment was backed by both spectroelectrochemical measurements and theoretical calculations. Analysis of the time evolution of these features afforded rate constants of 6.6×10^{11} and $1.0 \times 10^{10}\ s^{-1}$ for the charge separation and charge recombination dynamics, respectively. This is the first example of a fullerene fragment mimicking the charge transfer behavior of C_{60}, which paves the way to the study of other related known fullerene fragments, thus opening a new avenue for these electronically less-known carbon-based materials.

Received: November 6, 2013
Published online: January 22, 2014

Keywords: density functional calculations · donor-acceptor systems · fullerenes · photoinduced electron transfer · supramolecular chemistry

[1] J. L. Delgado, M. A. Herranz, N. Martín, *J. Mater. Chem.* **2008**, *18*, 1417 – 1426.
[2] a) N. Martín, *Chem. Commun.* **2006**, 2093 – 2104; b) J. Delgado, S. Filippone, F. Giacalone, M. Herranz, B. Illescas, E. M. Pérez, N. Martín, *Top. Curr. Chem.* **2013**, *320-331*, 1 – 64.
[3] *Carbon Nanotubes And Related Structures: Synthesis Characterization, Functionalization, And Applications* (Eds.: D. M. Guldi, N. Martín), Wiley-VCH, Weinheim, **2010**.
[4] a) M. J. Allen, V. C. Tung, R. B. Kaner, *Chem. Rev.* **2010**, *110*, 132 – 145; b) C. N. R. Rao, A. K. Sood, K. S. Subrahmanyam, A. Govindaraj, *Angew. Chem.* **2009**, *121*, 7890 – 7916; *Angew. Chem. Int. Ed.* **2009**, *48*, 7752 – 7777; c) A. K. Geim, *Science* **2009**, *324*, 1530 – 1534; d) A. K. Geim, K. S. Novoselov, *Nat. Mater.* **2007**, *6*, 183 – 191.
[5] a) N. Martín, L. Sánchez, M. A. Herranz, B. Illescas, D. M. Guldi, *Acc. Chem. Res.* **2007**, *40*, 1015 – 1024; b) D. Wróbel, A. Graja, *Coord. Chem. Rev.* **2011**, *255*, 2555 – 2577; c) S. Fukuzumi, T. Kojima, *J. Mater. Chem.* **2008**, *18*, 1427 – 1439; d) H. Imahori, *Org. Biomol. Chem.* **2004**, *2*, 1425 – 1433.
[6] a) G. Dennler, M. C. Scharber, C. J. Brabec, *Adv. Mater.* **2009**, *21*, 1323 – 1338; b) M. Helgesen, R. Søndergaard, F. C. Krebs, *J. Mater. Chem.* **2010**, *20*, 36 – 60; c) C. J. Brabec, S. Gowrisanker, J. J. M. Halls, D. Laird, S. Jia, S. P. Williams, *Adv. Mater.* **2010**, *22*, 3839 – 3856; d) H. Hoppe, N. S. Sariciftci, *J. Mater. Chem.* **2006**, *16*, 45 – 61; e) J. L. Delgado, P.-A. Bouit, S. Filippone, M. A. Herranz, N. Martín, *Chem. Commun.* **2010**, *46*, 4853 – 4865.
[7] a) J. M. Schnorr, T. M. Swager, *Chem. Mater.* **2011**, *23*, 646 – 657; b) C. Wang, K. Takei, T. Takahashi, A. Javey, *Chem. Soc. Rev.* **2013**, *42*, 2592 – 2609; c) S. Park, M. Vosguerichian, Z. Bao, *Nanoscale* **2013**, *5*, 1727 – 1752; d) S. N. Kim, J. F. Rusling, F. Papadimitrakopoulos, *Adv. Mater.* **2007**, *19*, 3214 – 3228.
[8] a) S. Bae, H. Kim, Y. Lee, X. Xu, J.-S. Park, Y. Zheng, J. Balakrishnan, T. Lei, H. R. Kim, Y. I. Song, Y.-J. Kim, K. S. Kim, B. Oezyilmaz, J.-H. Ahn, B. H. Hong, S. Iijima, *Nat. Nanotechnol.* **2010**, *5*, 574 – 578; b) X. Li, Y. Zhu, W. Cai, M. Borysiak, B. Han, D. Chen, R. D. Piner, L. Colombo, R. S. Ruoff, *Nano Lett.* **2009**, *9*, 4359 – 4363; c) K. S. Kim, Y. Zhao, H. Jang, S. Y. Lee, J. M. Kim, K. S. Kim, J.-H. Ahn, P. Kim, J.-Y. Choi, B. H. Hong, *Nature* **2009**, *457*, 706 – 710; d) X. Wang, L. Zhi, K. Müllen, *Nano Lett.* **2008**, *8*, 323 – 327.
[9] a) C.-H. Lu, H.-H. Yang, C.-L. Zhu, X. Chen, G.-N. Chen, *Angew. Chem.* **2009**, *121*, 4879 – 4881; *Angew. Chem. Int. Ed.* **2009**, *48*, 4785 – 4787; b) J. T. Robinson, F. K. Perkins, E. S. Snow, Z. Wei, P. E. Sheehan, *Nano Lett.* **2008**, *8*, 3137 – 3140; c) F. Schedin, A. K. Geim, S. V. Morozov, E. W. Hill, P. Blake, M. I. Katsnelson, K. S. Novoselov, *Nat. Mater.* **2007**, *6*, 652 – 655.
[10] a) Y. Zhu, S. Murali, M. D. Stoller, K. J. Ganesh, W. Cai, P. J. Ferreira, A. Pirkle, R. M. Wallace, K. A. Cychosz, M. Thommes, D. Su, E. A. Stach, R. S. Ruoff, *Science* **2011**, *332*, 1537 – 1541; b) K. Zhang, L. L. Zhang, X. S. Zhao, J. Wu, *Chem. Mater.* **2010**, *22*, 1392 – 1401; c) Y. Wang, Z. Shi, Y. Huang, Y. Ma, C. Wang, M. Chen, Y. Chen, *J. Phys. Chem. C* **2009**, *113*, 13103 – 13107.
[11] H. Hu, Z. Zhao, W. Wan, Y. Gogotsi, J. Qiu, *Adv. Mater.* **2013**, *25*, 2219 – 2223.
[12] X. Huang, Z. Yin, S. Wu, X. Qi, Q. He, Q. Zhang, Q. Yan, F. Boey, H. Zhang, *Small* **2011**, *7*, 1876 – 1902.
[13] M. A. Petrukhina, L. T. Scott, *Fragments of Fullerenes and Carbon Nanotubes: Designed Synthesis, Unusual Reactions, and Coordination Chemistry*, Wiley, Hoboken, **2012**, p. 413.
[14] a) S. Mizyed, P. Georghiou, M. Bancu, B. Cuadra, A. K. Rai, P. Cheng, L. T. Scott, *J. Am. Chem. Soc.* **2001**, *123*, 12770 – 12774; b) P. E. Georghiou, A. H. Tran, S. Mizyed, M. Bancu, L. T. Scott, *J. Org. Chem.* **2005**, *70*, 6158 – 6163; c) L. N. Dawe, T. A. AlHujran, H.-A. Tran, J. I. Mercer, E. A. Jackson, L. T. Scott, P. E. Georghiou, *Chem. Commun.* **2012**, *48*, 5563 – 5565.
[15] E. M. Pérez, M. Sierra, L. Sánchez, M. R. Torres, R. Viruela, P. M. Viruela, E. Ortí, N. Martín, *Angew. Chem.* **2007**, *119*, 1879 – 1883; *Angew. Chem. Int. Ed.* **2007**, *46*, 1847 – 1851.
[16] a) G. Mehta, G. Panda, P. V. V. S. Sarma, *Tetrahedron Lett.* **1998**, *39*, 5835 – 5836; b) S. Hagen, M. S. Bratcher, M. S. Erickson, G. Zimmermann, L. T. Scott, *Angew. Chem.* **1997**, *109*, 407 – 409; *Angew. Chem. Int. Ed. Engl.* **1997**, *36*, 406 – 408; c) A. H. Abdourazak, Z. Marcinow, A. Sygula, R. Sygula, P. W. Rabideau, *J. Am. Chem. Soc.* **1995**, *117*, 6410 – 6411.
[17] M. A. Petrukhina, K. W. Andreini, L. Peng, L. T. Scott, *Angew. Chem.* **2004**, *116*, 5593 – 5597; *Angew. Chem. Int. Ed.* **2004**, *43*, 5477 – 5481.
[18] A. Dalla Cort, L. Mandolini, C. Pasquini, L. Schiaffino, *New J. Chem.* **2004**, *28*, 1198 – 1199.

[19] H. Isla, B. Grimm, E. M. Pérez, M. Rosario Torres, M. A. Herranz, R. Viruela, J. Aragó, E. Ortí, D. M. Guldi, N. Martín, *Chem. Sci.* **2012**, *3*, 498 – 508.
[20] a) Y. Zhang, W. Yang, *Phys. Rev. Lett.* **1998**, *80*, 890 – 890; b) S. Grimme, J. Antony, S. Ehrlich, H. Krieg, *J. Chem. Phys.* **2010**, *132*, 154104 – 154118.
[21] W. Hujo, S. Grimme, *J. Chem. Theory Comput.* **2011**, *7*, 3866 – 3871.
[22] F. G. Brunetti, H. Isla, J. Aragó, E. Ortí, E. M. Pérez, N. Martín, *Chem. Eur. J.* **2013**, *19*, 9843 – 9848.

